Separation Science and Technology
Publication details, including instructions for authors and subscription information:
http://www.informaworld.com/smpp/title~content=t713708471

Concentration Polarization Model for Hollow-Fiber Membrane Ultrafiltration

Ho-Ming Yeh[a]; Tung-Wen Cheng[b]
[a] DEPARTMENT OF CHEMICAL ENGINEERING, TAMKANG UNIVERSITY, TAMSUI, TAIWAN, REPUBLIC OF CHINA [b] DEPARTMENT OF CHEMICAL ENGINEERING, NATIONAL TAIWAN UNIVERSITY, TAIPEI, TAIWAN, REPUBLIC OF CHINA

To cite this Article Yeh, Ho-Ming and Cheng, Tung-Wen(1994) 'Concentration Polarization Model for Hollow-Fiber Membrane Ultrafiltration', Separation Science and Technology, 29: 4, 497 — 512
To link to this Article: DOI: 10.1080/01496399408002158
URL: http://dx.doi.org/10.1080/01496399408002158

SEPARATION SCIENCE AND TECHNOLOGY, **29**(4), pp. 497–512, 1994

Concentration Polarization Model for Hollow-Fiber Membrane Ultrafiltration

HO-MING YEH
DEPARTMENT OF CHEMICAL ENGINEERING
TAMKANG UNIVERSITY
TAMSUI, TAIWAN, REPUBLIC OF CHINA

TUNG-WEN CHENG
DEPARTMENT OF CHEMICAL ENGINEERING
NATIONAL TAIWAN UNIVERSITY
TAIPEI, TAIWAN, REPUBLIC OF CHINA

ABSTRACT

The concentration polarization model has been applied to analyze the permeate flux of hollow-fiber membrane ultrafiltration. Comparison of theoretical prediction with experimental data has been made under various transmembrane pressures, feed velocities, and solution concentrations. Both theoretical prediction and experimental results show that average permeate flux increases as transmembrane pressure or feed velocity increases, but decreases when solution concentration increases.

Key Words. Concentration polarization model; Hollow fiber; Ultrafiltration; Permeate flux

INTRODUCTION

Ultrafiltration has now assumed prominence as a practical industrial process for the concentration, purification, or dewatering of macromolecular and colloidal species in solution. One of the common ultrafiltration designs is the hollow-fiber configuration in which the membrane is formed on the inside of tiny polymer cylinders that are then bundled and potted into a tube-and-shell arrangement.

The rapid development of this process was made possible by the advent of anisotropic, high-flux membranes capable of distinguishing among molecular and colloidal species in the 10 Å to 10 μm size range. Since this process is a pressure-driven membrane separation, the pressure applied to the working fluid provides the driving potential to force the solvent to flow through the membrane. Typical driving pressures for ultrafiltration systems are in the range of 10 to 100 psi. For a small applied pressure, the solvent flux through a membrane is observed to be proportional to the applied pressure. However, as the pressure is increased further, the flux begins to drop below that which would result from a linear flux-pressure behavior. Eventually a limiting flux is reached where any further pressure increase no longer results in any increase in flux. The reason for the existence of a limiting flux is that the high-flux characteristics of these membranes result in rapid convection of retained solutes to the membrane surface, leading to the well-known phenomena of concentration polarization. Under high-pressure operation, the concentration at the membrane surface can even rise to the point of incipient gel precipitation, forming a dynamic secondary membrane on top of the primary structure. Furthermore, concentrated solutions of macromolecules have quite an appreciable osmotic pressure. At the high concentrations found in ultrafiltration polarization layers, the osmotic pressure can even be of the same order of magnitude as the applied pressures generally used in ultrafiltration.

Permeate flux of ultrafiltration is always analyzed by use of one of following models: the gel-polarization model (1–8), the osmotic-pressure model (9–17), or the resistance-in-series model (17, 18). In this study, the concentration polarization model for analyzing the permeate flux of hollow-fiber ultrafiltration will be introduced. The effects of various parameters on permeate flux will also be discussed.

THEORY

The model was developed to simulate forced-convection ultrafiltration in a horizontal hollow-fiber membrane system. The feed-concentrate stream in the inside of the membrane tubes is laminar, and the mass density, viscosity, and solute diffusivity are assumed to be constant. We also assume that the thickness of the concentration-polarization layer near the tube wall is small, and that this boundary layer may be considered to be a flat plate.

The Governing Equations

Referring to Fig. 1, an integral equation for solute balance within the concentration boundary layer may be obtained as

$$c_0 \left\{ \rho v_m(z)dz + \frac{d}{dz}\left[\int_{r_m - \delta(z)}^{r_m} \rho u(z, r)dr \right] dz \right\} = \frac{d}{dz}\left[\int_{r_m - \delta(z)}^{r_m} c(z, r)\rho u(z, r)dr \right] dz \tag{1}$$

or it may be rewritten as

$$\frac{d}{dz}\int_{r_m - \delta(z)}^{r_m} u(z, r)[c(z, r) - c_0]dr - c_0 v_m(z) = 0 \tag{2}$$

Integrating Eq. (2) with respect to z and using the boundary condition $c = c_0$ at $z = 0$, the above equation becomes

$$\int_0^1 u(\xi, \zeta)[c(\xi, \zeta) - c_0]\delta(\xi)d\zeta = c_0 L v_{m0} \int_0^\xi V(\xi)d\xi \tag{3}$$

where

$$\zeta = y/\delta \tag{4}$$

$$y = r_m - r \tag{5}$$

$$V(\xi) = v_m/v_{m0} \tag{6}$$

$$\xi = z/L \tag{7}$$

in which v_{m0} denotes the permeate flux at the entrance of hollow fibers.

Yuan and Finkelstein (19) used a perturbation technique to solve the Navier–Stokes equations and obtain the steady-state z-component velocity profile for laminar flow through a porous tube. For small values of permeation velocity and tube radius that are appropriate to this work, their result reduces to the following equations:

$$\frac{u(z, r)}{u_0} = 2\left[1 - 2\left(\frac{v_m(z)z}{u_0 r_m}\right)\right]\left[1 - \left(\frac{r}{r_m}\right)^2\right] \tag{8}$$

$$\frac{v(z, r)}{v_m(z)} = \left[2\left(\frac{r}{r_m}\right) - \left(\frac{r}{r_m}\right)^3\right] \tag{9}$$

The axial velocity distribution expressed by Eq. (8) can be rewritten as

$$\frac{u(\xi, \zeta)}{u_0} = 2\left[1 - \left(\frac{2}{\gamma}\right)V(\xi)\xi\right]\left[2\left(\frac{\delta(\xi)}{r_m}\right)\zeta - \left(\frac{\delta(\xi)}{r_m}\right)^2 \zeta^2\right] \tag{10}$$

where

$$\gamma = u_0 r_m / v_{m0} L \tag{11}$$

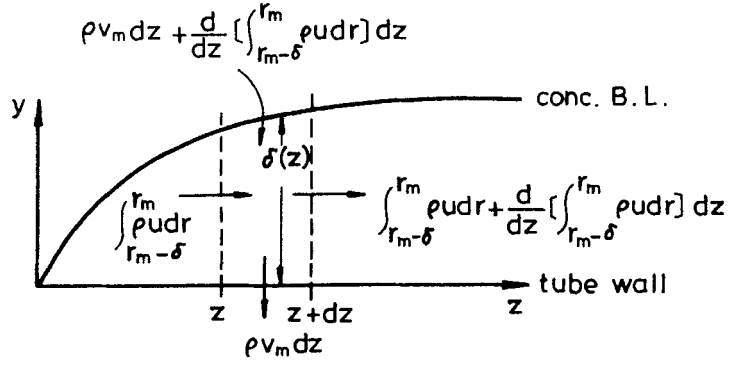

(a) Total balance

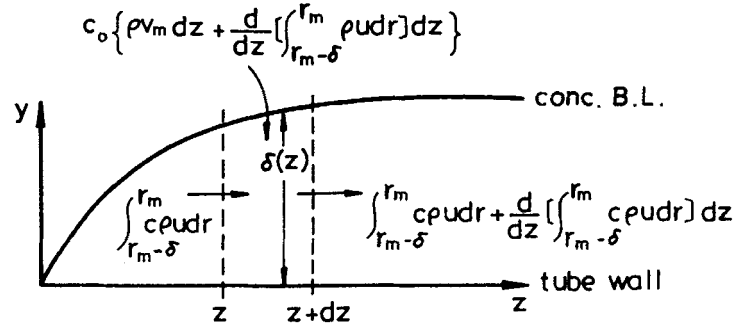

(b) Solute balance

FIG. 1 Mass balances within the concentration boundary layer.

Since the thickness of concentration boundary layer is very thin, within it the concentration profile may be assumed to be the following function of ζ:

$$c(\xi, \zeta) - c_0 = [c_m(\xi) - c_0](1 - \zeta)^2 \tag{12}$$

It should be noted that the above equation satisfies the boundary condition $c = c_0$ and $\partial c/\partial\zeta = 0$ at the boundary layer, $\zeta = 1$, while $c = c_m$ at $\zeta = 0$. By substitution of Eqs. (10) and (12) into Eq. (3), one obtains

$$2\gamma\left[1 - \left(\frac{2}{\gamma}\right)V(\xi)\xi\right][C(\xi) - 1]\left(\frac{\delta(\xi)}{r_m}\right)\left[\frac{1}{6}\left(\frac{\delta(\xi)}{r_m}\right) - \frac{1}{30}\left(\frac{\delta(\xi)}{r_m}\right)^2\right] = \int_0^\xi V(\xi)d\xi \tag{13}$$

where

$$C(\xi) = c_m(\xi)/c_0 \tag{14}$$

Making a solute mass balance at the membrane surface where perfect solute rejection occurs, we have

$$v_m(z)c_m(z) = D\left.\frac{\partial c(z, r)}{\partial r}\right|_{r=r_m} \quad \text{or} \quad v_m(\xi)c_m(\xi) = -\frac{D}{\delta(\zeta)}\left.\frac{\partial c(\xi, \zeta)}{\partial\zeta}\right|_{\zeta=0} \tag{15}$$

Substitution of Eq. (12) into Eq. (15) yields the thickness of the concentration boundary layer as

$$\frac{\delta(\xi)}{r_m} = \frac{2\Lambda[C(\xi) - 1]}{C(\xi)V(\xi)} \tag{16}$$

where

$$\Lambda = D/v_{m0}r_m \tag{17}$$

By substitution of Eq. (16) into Eq. (13), one obtains the dimensionless concentration distribution of solute at the membrane surface, $C(\xi)$, relating with the dimensionless solvent permeate flux, $V(\xi)$, as

$$\frac{2\gamma(C(\xi) - 1)^3\Lambda^2}{C(\xi)^2V(\xi)^2}\left[1 - 2V(\xi)\left(\frac{\xi}{\gamma}\right)\right]\left[\frac{1}{6} - \frac{1}{15}\frac{\Lambda(C(\xi) - 1)}{C(\xi)V(\xi)}\right] = \int_0^\xi V(\xi)d\xi \tag{18}$$

In membrane separation processes, solutes that are rejected by the membrane accumulate on the membrane surface. The concentration of solutes on the membrane surface is always higher than in the bulk solution. This is the so-called concentration polarization phenomenon. Complete solute rejection on the membrane surface will be assumed in this study.

At steady state, the quantity of solutes conveyed to the membrane is equal to those that transfer back by convection. Consequently, the following solute balance at the membrane surface is reached.

$$v_m(\xi)c_m(\xi) = \dot{k}(\xi)[c_m(\xi) - c_0] \tag{19}$$

Since the convective mass transfer rate of solute from the membrane surface to the bulk fluid is generally high, a high mass-transfer rate is considered in Eq. (19). According to film theory, the coefficient of high mass-transfer rate $\dot{k}$ is related with that of low mass-transfer rate k as (20)

$$\dot{k}(\xi) = \frac{v_m(\xi)}{1 - \exp[-v_m(\xi)/k(\xi)]} \tag{20}$$

Combination of Eqs. (19) and (20) for eliminating $\dot{k}$ yields

$$C(\xi) = \frac{c_m(\xi)}{c_0} = \exp[v_m(\xi)/k(\xi)] = \exp[v_{m0}(\xi)/k(\xi)]V(\xi) \tag{21}$$

or

$$V(\xi) = [k(\xi)/v_{m0}(\xi)] \ln C(\xi) \tag{22}$$

The Graetz solution (21) for convective heat transfer in laminar flow channels, suitably modified for mass transfer, may be used to evaluate the mass-transfer coefficient k. The Graetz solution gives

$$k(\xi) = 1.08\left(\frac{u_b D^2}{2r_m z}\right)^{1/3} = 0.86\left(\frac{u_b D^2}{r_m L \xi}\right)^{1/3} \tag{23}$$

Taking the overall balance over the tube section from $z = 0$ to $z = z$, one obtains

$$Q = Q_0 - 2\pi r_m \int_0^z v_m(z)\, dz \tag{24}$$

This can be written in dimensionless form as

$$\frac{u_b(\xi)}{u_0} = 1 - \left(\frac{2}{\gamma}\right)\int_0^\xi V(\xi)\, d\xi \tag{25}$$

From Eqs. (23) and (25), we have

$$\begin{aligned}\frac{v_{m0}}{k(\xi)} &= 1.16 v_{m0}\left(\frac{r_m L \xi}{u_b D^2}\right)^{1/3} \\ &= 1.16\left[\left(\frac{u_0}{u_b}\right)\left(\frac{v_{m0}L}{u_0 r_m}\right)\left(\frac{v_{m0}r_m}{D}\right)^2 \xi\right]^{1/3} \\ &= 1.16\gamma^{1/3}\Lambda^{-2/3}\xi^{1/3}\left[1 - \frac{2}{\gamma}\int_0^\xi V(\xi)\, d\xi\right]^{-1/3}\end{aligned} \tag{26}$$

Substitution of Eq. (26) into Eq. (21) results in

$$C(\xi) = \exp\left[V(\xi)\left\{1.16\gamma^{1/3}\Lambda^{-2/3}\xi^{1/3}\left[1 - \frac{2}{\gamma}\int_0^{\xi} V(\xi)\,d\xi\right]^{-1/3}\right\}\right] \quad (27)$$

which is the second relation between solvent permeate flux and solute concentration at the membrane surface. Finally, the dimensionless solvent permeate flux $V(\xi)$ and the dimensionless solute concentration at membrane surface $C(\xi)$ may be obtained by solving Eqs. (18) and (27) simultaneously, as follows.

Permeate Fluxes

For simplicity, we assume that the dimensionless solvent permeate flux decays along the longitudinal position as

$$V(\xi) = 1 - b\xi(2 - \xi) \quad (28)$$

in which b is a constant to be determined. In addition to the inlet condition

$$V = 1 \quad \text{at} \quad \xi = 0 \quad (29)$$

Eq. (28) also satisfies the approximate outlet condition shown by the experimental results (15):

$$\partial V/\partial\xi = 0 \quad \text{at} \quad \xi = 1 \quad (30)$$

Substituting Eq. (28) into Eqs. (18) and (27), and then letting $\xi = 1$, two algebraic equations for b and C_1 (value of C at $\xi = 1$) are obtained:

$$\frac{8\gamma(C_1 - 1)^3\Lambda^2}{C_1^2(1 - b)^2}\left[1 - \frac{2 - (1 - b)}{\gamma}\right]\left[\frac{1}{6} - \frac{1}{15}\frac{\Lambda(C_1 - 1)}{C_1(1 - b)}\right] = 1 - \frac{2b}{3} \quad (31)$$

$$C_1 = \exp\left[1.16\gamma^{1/3}\Lambda^{-2/3}(1 - b)\left\{1 - \frac{2}{\gamma}\left(1 - \frac{2b}{3}\right)\right\}\right]^{-1/3} \quad (32)$$

Thus, b and C_1 can be determined by solving Eqs. (31) and (32) simultaneously. The results are shown in Fig. 2 with γ and Λ as parameters. It is seen from Fig. 2 that if γ is small, the solute concentration on the membrane surface at the outlet can reach several hundred times that at the inlet, leading to high resistance to concentration polarization at the outlet.

The average solvent permeate flux through a whole hollow fiber may be defined as

$$\bar{v}_m = \frac{1}{L}\int_0^L v_m(z)\,dz \quad (33)$$

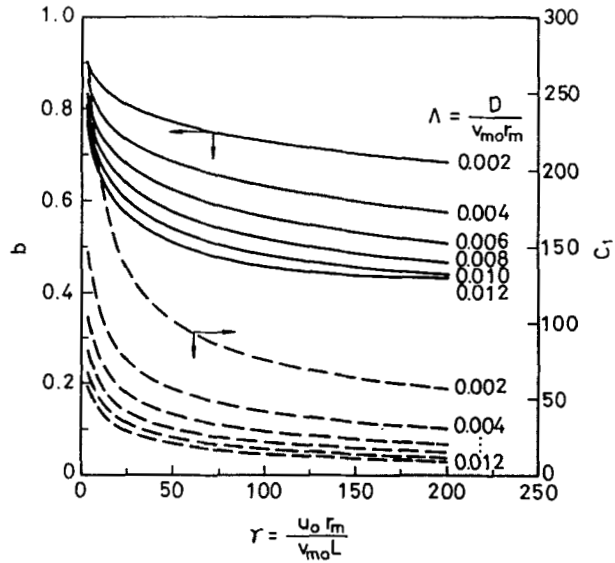

FIG. 2 Calculated values of b and C_1.

or, in dimensionless form,

$$\overline{V} = \frac{\overline{v}_m}{v_{m0}} = \int_0^1 V(\xi)\, d\xi \tag{34}$$

By substitution of Eq. (28) into Eq. (34), we have

$$\overline{V} = 1 - \frac{2b}{3} \tag{35}$$

The graphical representation of $\overline{V}$ is given in Fig. 3. It is seen from this figure that average permeate flux increases as the diffusion coefficient D increases. This is because an increase of diffusivity will increase the mass-transfer coefficient, resulting in increasing the permeate flux as shown in Eqs. (22) and (23). The permeate flux also increases as u_0 increases or as L decreases.

Comparison of Theoretical Prediction with Experimental Results

The theoretical prediction of average permeate flux $\overline{v}_m$ will be compared with the experimental results obtained by Cheng (22, 23). Cheng employed

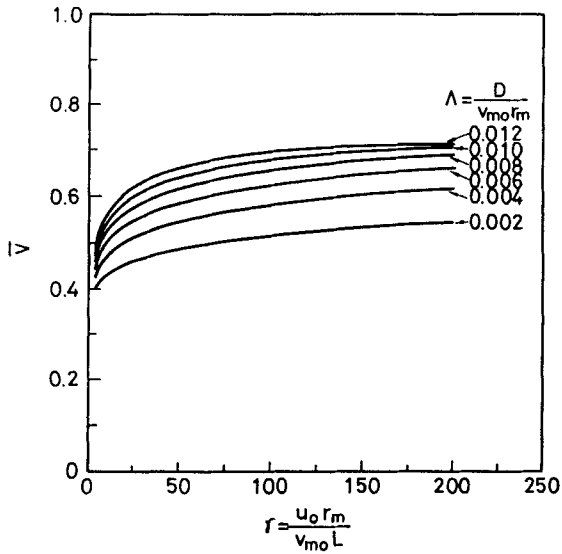

FIG. 3 Calculated values of $\bar{V}$.

an Amicon model H1P 30-20 hollow-fiber cartridge ($r_m = 2.5 \times 10^{-4}$ m, $L = 0.153$ m, effective membrane area = 600 cm^2) made of polysulfone for experimental studies on membrane ultrafiltration of aqueous solutions of Dextran T500 (Pharmacia, $M_n = 170{,}300$ and $M_w = 503{,}000$) at 25°C. The flow sheet of the ultrafiltration apparatus used in Cheng's work is shown in Fig. 4. The experiments will be described briefly: The tested solute was more than 99% retained by the membrane used. The solvent was ion exchange pure water. The feed solution was circulated by a high-pressure pump with a variable speed motor (L-07553-20, Cole-Parmer Co., Chicago, Illinois, USA) and the feed flow was measured with a flowmeter (L-03217-34, Cole-Parmer Co.). The pressure was measured by a pressure transmitter (model 891.14.425, Wika).

The feed solution concentrations were 0.1, 0.2, 0.5, 1.0, and 2.0 wt% dextran T500, the feed flow velocities were 0.051, 0.102, 0.204, 0.306 m/s, and the feed inlet pressures were 30, 50, 70, 100, and 140 kPa. During a run, both permeate and retentate were recycled back to the feed tank to keep the feed concentration constant. After each solution run, the membrane module was cleaned by a combination of high circulation and back-flushing with pure water. The experimental results are shown in Figs. 5–9.

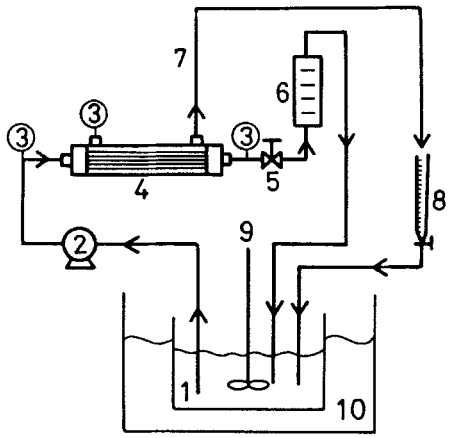

1 . feed tank
2 . pump
3 . pressure gauge
4 . hollow fiber module
5 . pressure control valve
6 . flow meter
7 . permeate
8 . collector
9 . stirrer
10. thermostat

FIG. 4 Flow diagram of ultrafiltration apparatus.

For theoretical prediction, the diffusivity of Dextran T500 in aqueous solution at 25°C may be estimated by the following empirical equation (24):

$$D \times 10^{11} = 1.204 + 2.875 \times 10^{-1} c_0 - 5.042 \times 10^{-3} c_0^2 + 2.838 \times 10^{-5} c_0^3 \tag{36}$$

in which the unit of concentration has been changed from g/mL to wt%. The values of v_{m0} could be calculated from the correlation equation obtained in Cheng's works. The correlation equation for v_{m0} is

$$v_{m0} = \frac{\Delta P_0}{2.42\times 10^9 + 7.49\times 10^8 u_0^{-0.15} e^{0.87 c_0} + 1.56\times 10^5 u_0^{-0.34} c_0^{0.42} \Delta P_0} \tag{37}$$

Thus, the theoretical values of $\bar{v}_m$ are calculated from Eqs. (35), (36), and (37) coupled with the use of Fig. 2. The theoretical results are also presented in Figs. 5–9 for comparison.

It is found from Figs. 5–9 that the deviation of theoretical values from the experimental data increases as the feed velocity or transmembrane pressure increases, or when the solution concentration decreases. The

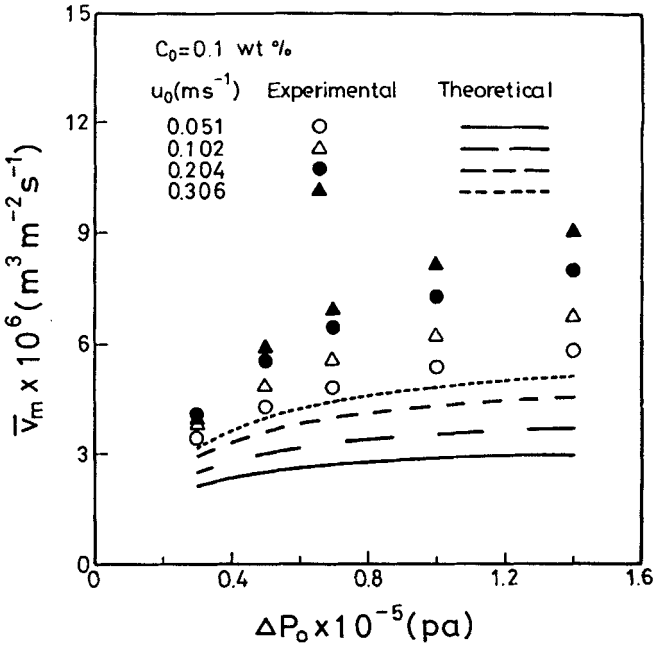

FIG. 5 Comparison of theoretical values with experimental results for c_0 = 0.1 wt%.

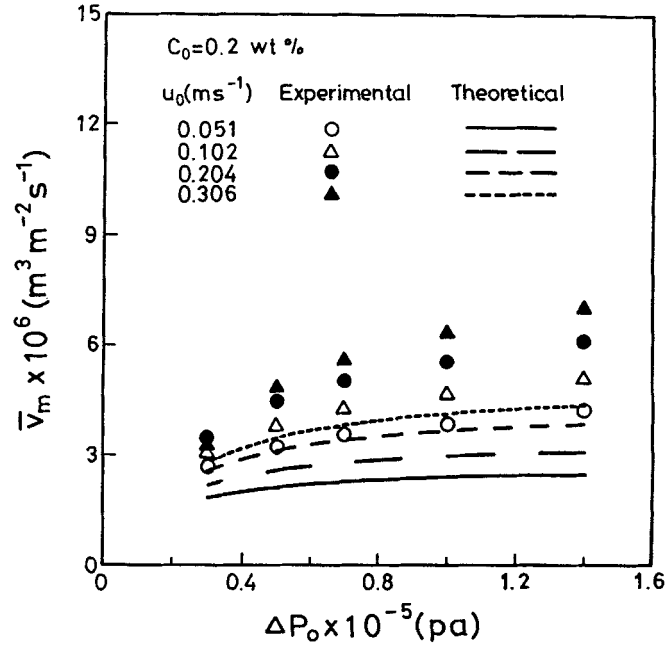

FIG. 6 Comparison of theoretical values with experimental results for c_0 = 0.2 wt%.

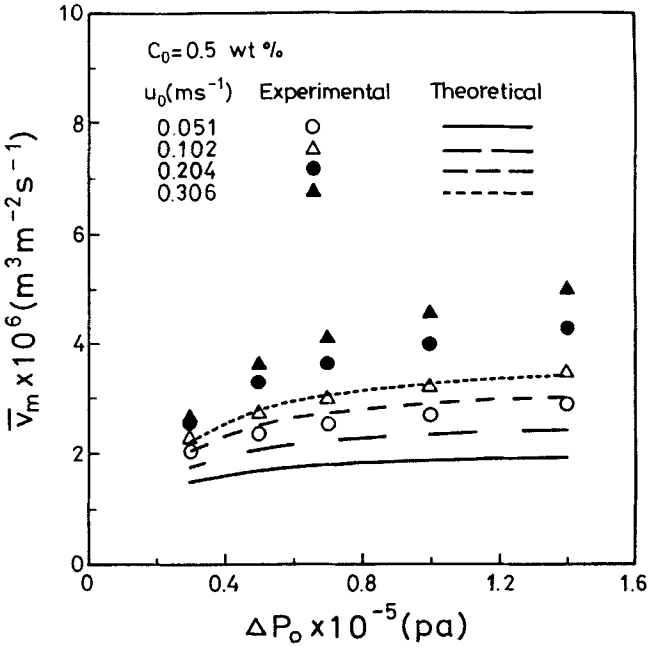

FIG. 7 Comparison of theoretical values with experimental results for c_0 = 0.5 wt%.

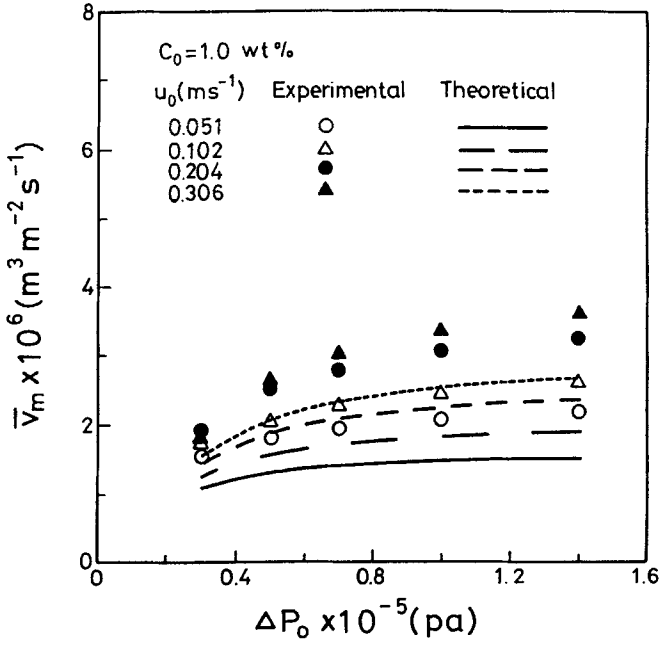

FIG. 8 Comparison of theoretical values with experimental results for c_0 = 1.0 wt%.

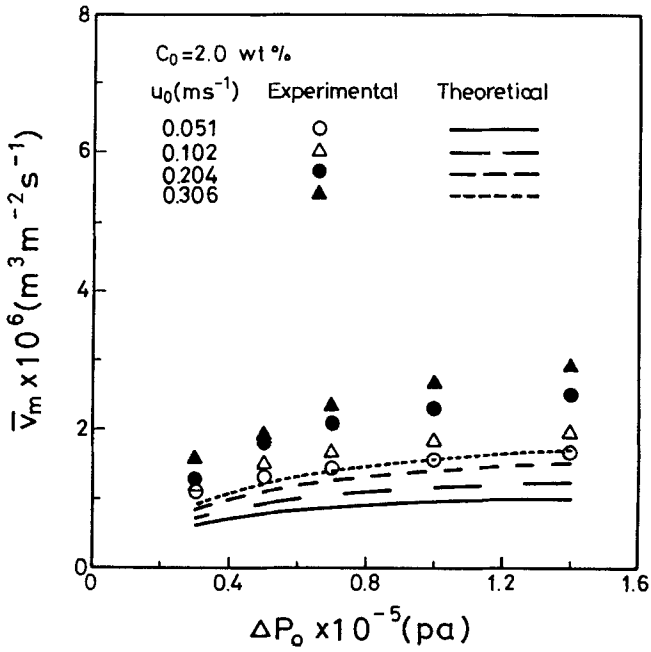

FIG. 9 Comparison of theoretical values with experimental results for c_0 = 2.0 wt%.

reasons for the occurrence of this deviation may be the following unsuitable assumptions: flat plate (i.e., δ/r_m is small), constant diffusivity, choice of assumed forms (Eqs. 12 and 28), and choice of the boundary condition (Eq. 30).

CONCLUSIONS

A concentration polarization model for analyzing the permeate flux of hollow-fiber membrane ultrafiltration has been introduced. First, a dimensionless integral equation, Eq. (18), was derived from the solute balance. In this equation the solute concentration on the membrane surface, $C(\xi)$, is related to the solvent permeate flux, $V(\xi)$, and they are the unknown functions to be determined. Another relation, between permeate flux and solute concentration on membrane surface, Eq. (27), has also been derived from the concept of concentration polarization. Mathematically, the distributions of permeate flux and solute concentration on a membrane surface may be obtained by solving Eqs. (18) and (27) simultaneously.

For simplicity, an approximate solution for permeate-flux distribution was obtained by assuming it has a quadratic form, Eq. (28). The average permeate fluxes were thus calculated, and the results are presented in Figs. 5–9 for comparison with experimental data. Both theoretical prediction and experimental results show that the average permeate flux increases as the transmembrane pressure or feed velocity increases, but it decreases when the solution concentration increases.

It is also seen from Figs. 5–9 that theoretical prediction qualitatively agrees with experimental data. However, the deviation of theoretical values from the experimental data increases as the feed velocity or transmembrane pressure increases, or when the solution concentration decreases. It is believed that theoretical prediction may be improved if better forms of the assumed equations can been found.

SYMBOLS

b	constant defined in Eq. (28)
c	solute concentration (wt%)
c_0	inlet solute concentration (wt%)
$c_m(z)$	solute concentration at the membrane surface (wt%)
$C(\xi)$	dimensionless solute concentration, c_m/c_0
C_1	dimensionless solute concentration at outlet, $C(\xi = 1)$
D	diffusion coefficient ($m^2 \cdot s^{-1}$)
k	mass transfer coefficient for low mass-transfer rate ($m^3 \cdot m^{-2} \cdot s^{-1}$)
$\dot{k}(z)$	mass transfer coefficient for high mass-transfer rates ($m^3 \cdot m^{-2} \cdot s^{-1}$)
L	length of hollow fiber (m)
ΔP_0	transmembrane pressure at fiber inlet (Pa)
Q	volume rate of flow, $\pi r_m^2 u_b$ ($m^3 \cdot s^{-1}$)
Q_0	Q at the entrance ($m^3 \cdot s^{-1}$)
r	radial coordinate (m)
r_m	radius of hollow fiber (m)
$u(z, r)$	axial velocity ($m \cdot s^{-1}$)
u_0	mean axial velocity at fiber inlet ($m \cdot s^{-1}$)
$u_b(z)$	bulk axial velocity ($m \cdot s^{-1}$)
$v(z, r)$	radial velocity ($m \cdot s^{-1}$)
$v_m(z)$	membrane permeation flux ($m^3 \cdot m^{-2} \cdot s^{-1}$)
$\bar{v}_m$	mean membrane permeation flux defined in Eq. (33) ($m^3 \cdot m^{-2} \cdot s^{-1}$)
v_{m0}	membrane permeation flux at fiber inlet ($m^3 \cdot m^{-2} \cdot s^{-1}$)
$V(\xi)$	dimensionless membrane permeation flux, v_m/v_{m0}

$\overline{V}$	dimensionless mean membrane permeation flux, $\overline{v}_m/v_{m0}$
y	$r_m - r$(m)
z	axial coordinate (m)
γ	dimensionless parameter, $(u_0 r_m)/(v_{m0} L)$
$\delta(z)$	thickness of the concentration boundary layer (m)
ζ	y/δ
Λ	dimensionless parameter, $D/(v_{m0} r_m)$
ξ	z/L
ρ	density of solution ($kg \cdot m^{-3}$)

ACKNOWLEDGMENT

The authors wish to express their thanks to the Chinese National Science Council for financial aid.

REFERENCES

1. W. F. Blatt, A. Dravid, A. S. Michael, and L. Nelsen, "Solute Polarization and Cake Formation in Membrane Ultrafiltration: Causes, Consequences, and Control Techniques," in *Membrane Science and Technology* (J. E. Flinn, Ed.), Plenum Press, New York, 1970, pp. 47–97.
2. M. C. Porter, "Concentration Polarization with Membrane Ultrafiltration," *Ind. Eng. Chem., Prod. Res. Dev., 11*, 234 (1972).
3. R. B. Grieves, D. Bhattacharyya, W. G. Schomp, and J. L. Bewley, "Membrane Ultrafiltration of a Nonionic Surfactant," *AIChE J., 19*, 766 (1973).
4. J. J. S. Shen and R. F. Probstein, "On the Prediction of Limiting Flux in Laminar Ultrafiltration of Macromolecular Solutions," *Ind. Eng. Chem., Fundam., 16*, 459 (1977).
5. R. F. Probstein, W. Leung, and Y. Alliance, "Determination of Diffusivity and Gel Concentration in Macromolecular Solutions by Ultrafiltration," *J. Phy. Chem., 83*, 1228 (1979).
6. S. Nakao, T. Nomura, and S. Kumura, "Characteristics of Macromolecular Gel Layer Formed on Ultrafiltration Tubular Membrane," *AIChE J., 25*, 615 (1979).
7. A. G. Fane, C. J. D. Fell, and A. G. Waters, "The Relationship between Membrane Surface Pore Characteristics and Flux for Ultrafiltration Membranes," *J. Membr. Sci., 9*, 245 (1981).
8. A. G. Fane, "Ultrafiltration of Suspensions," *Ibid., 20*, 249 (1984).
9. J. G. Wijmans, S. Nakao, and C. A. Smolders, "Flux Limitation in Ultrafiltration: Osmotic Pressure Model and Gel Layer Model," *Ibid., 20*, 115 (1984).
10. A. A. Kozinski and E. N. Lightfoot, "Protein Ultrafiltration: A General Example of Boundary Layer Filtration," *AIChE J., 18*, 1030 (1972).
11. W. Leung and R. F. Probstein, "Low Polarization in Laminar Ultrafiltration of Macromolecular Solutions," *Ind. Eng. Chem., Fundam., 18*, 274 (1979).
12. R. P. Wendt, E. Klein, F. F. Holland, and K. E. Eberle, "Hollow Fiber Ultrafiltration of Calf Serum and Albumin in the Pregel Uniform-Wall-Flux Region," *Chem. Eng. Commun., 8*, 251 (1981).

13. S. Nakao and S. Kimura, "Models of Membrane Transport Phenomena and Their Applications for Ultrafiltration Data," *J. Chem. Eng. Jpn.*, *15*, 200 (1982).
14. C. Kleinstreuer and M. S. Paller, "Laminar Dilute Suspension Flows in Plate-and-Frame Ultrafiltration Units," *AIChE J.*, 529 (1983).
15. M. J. Clifton, N. Abidine, P. Aptel, and V. Sanchez, "Growth of the Polarization Layer in Ultrafiltration with Hollow-Fiber Membranes," *J. Membr. Sci.*, *21*, 233 (1984).
16. R. P. Ma, C. H. Gooding, and W. K. Alexander, "A Dynamic Model for Low-Pressure, Hollow-Fiber Ultrafiltration," *AIChE J.*, *31*, 1728 (1985).
17. H. Nabetani, M. Nakajima, A. Watanabe, S. Nakao, and S. Kimura, "Effects of Osmotic Pressure and Adsorption on Ultrafiltration of Ovalbumin," *AIChE J.*, *36*, 907 (1990).
18. B. H. Chiang and M. Cheryan, "Ultrafiltration of Skimmilk in Hollow Fibers," *J. Food Sci.*, *51*, 340 (1986).
19. S. W. Yuan and A. B. Finkelstein, "Laminar Pipe Flow with Injection and Suction through a Porous Wall," *Trans. ASME*, *78*, 719 (1956).
20. R. B. Bird, W. E. Stewart, and E. N. Lightfoot, *Transport Phenomena*, Wiley, New York, 1960, pp. 662–663.
21. L. Graetz, "Uber die Waermeleitungsfaehigkeit von Fluessigkeiten," *Ann. Phys. Chem.*, *18*, 79 (1883).
22. T. W. Cheng, "Hollow-Fiber Membrane Ultrafiltration," Ph.D. Thesis, National Taiwan University, Taipei, Taiwan, R.O.C., 1992.
23. H. M. Yeh and T. W. Cheng, "Resistance-in-Series for Membrane Ultrafiltration in Hollow Fibers of Tube-and-Shell Arrangement," *Sep. Sci. Technol.*, *28*, 1341 (1993).
24. J. G. Wijmans, S. Nakao, J. W. A. Van Den Berg, F. R. Troelstra and C. A. Smolders, "Hydrodynamic Resistance of Concentration Polarization Boundary Layers in Ultrafiltration," *J. Membr. Sci.*, *22*, 117 (1985).

Received by editor June 24, 1993